Chemical Science

ROYAL SOCIETY OF CHEMISTRY

EDGE ARTICLE

View Article Online
View Journal | View Issue

Cite this: *Chem. Sci.*, 2025, **16**, 824

All publication charges for this article have been paid for by the Royal Society of Chemistry

Received 13th September 2024
Accepted 14th November 2024

DOI: 10.1039/d4sc06219a

rsc.li/chemical-science

Ruthenaelectro-catalyzed C–H phosphorylation: *ortho* to *para* position-selectivity switch†

Xue-Ya Gou,‡ João C. A. Oliveira, ‡ Shan Chen, Simon L. Homölle, Sven Trienes, Tristan von Münchow, Bo-Sheng Zhang and Lutz Ackermann *

The position-selective C–H bond activation of arenes has long been a challenging topic. Herein, we report an expedient ruthenium-electrocatalyzed site-selective *ortho*-C–H phosphorylation of arenes driven by electrochemical hydrogen evolution reaction (HER), avoiding stoichiometric amounts of chemical redox-waste products. This strategy paved the way to achieve unprecedented ruthenaelectro-catalyzed *para*-C–H phosphorylation with excellent levels of site-selectivity. This electrocatalytic approach was characterized by an ample substrate scope with a broad range of arenes containing N-heterocycles, as well as several aryl/alkylphosphine oxides were well tolerated. Moreover, late-stage C–H phosphorylation of medicinal relevant drugs could also be achieved. DFT mechanistic studies provided support for an unusual ruthenium(III/IV/II) regime for the *ortho*-C–H phosphorylation.

Introduction

Organophosphorus compounds have been widely employed in organic synthesis,[1] medicinal chemistry,[2] material sciences,[3] as well as prominent ligands[4] in catalytic reactions. The presence of a phosphoryl group in target molecules has often been reported to enhance their physical-chemical properties, such as their hydrophilicity, thereby improving their solubility and tolerance in biological systems.[5] Compounds bearing phosphine oxide motifs have revealed potential in decreasing inflammation, reducing blood sugar, and even anti-HIV activity.[6] Additionally, phosphorylated heteroarenes have been reported as the one of the main components in phosphorescent OLEDs, due to their excellent luminescence properties (Scheme 1a).[7] In this context, the development of novel and efficient strategies for the construction of aromatic C–P bonds poses great significance.

Transition metal-catalyzed C–H activation has emerged as a powerful tool in modern synthesis.[8] Direct C–H phosphorylation of arenes has proven to be challenging due to the strong coordination ability of the phosphine reagents, which often leads to catalyst deactivation. To overcome this drawback, distinct strategies have been developed. These involve the slow addition of the phosphine reagents,[9] the use of masked phosphine reagents, which slowly release the active phosphine

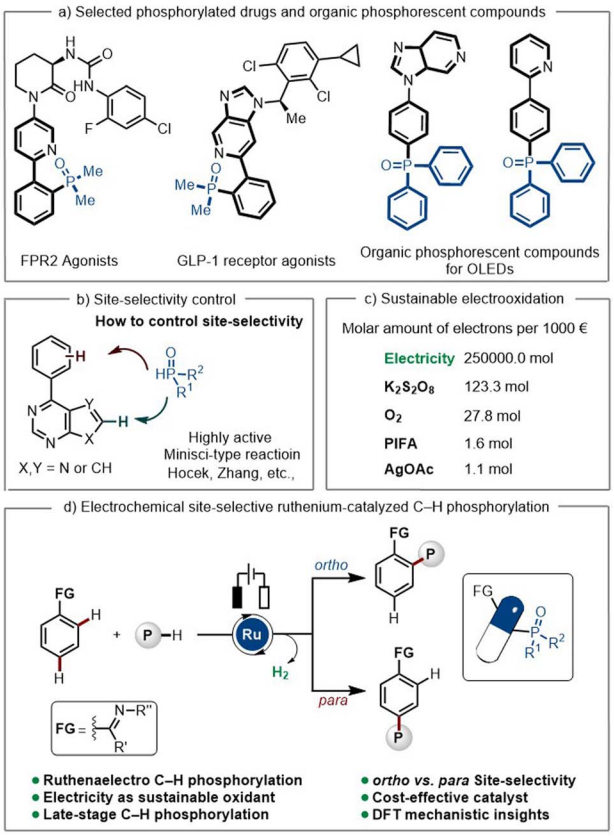

Scheme 1 Electrochemical ruthenium-catalyzed site-selective C–H phosphorylation.

Wöhler Research Institute for Sustainable Chemistry (WISCh), Georg-August-Universität, Tammannstraße 2, 37077 Göttingen, Germany. E-mail: Lutz.Ackermann@chemie.uni-goettingen.de

† Electronic supplementary information (ESI) available. See DOI: https://doi.org/10.1039/d4sc06219a

‡ These authors contributed equally.

compounds[10] or their sequential addition.[11] However, these approaches involve the use of stoichiometric amounts of chemical oxidants, which strongly jeopardizes the sustainability of the overall approaches. On a different note, phosphine radical-based strategies for the synthesis of aryl phosphonyl compounds have been limited to electron-rich arenes, with poor position-selectivity.[12] Furthermore, Minisci-type reactivity of nitrogen-containing heterocycles based on phosphine radicals is predominant,[13] rendering phosphorylation at remote position difficult.

Ruthenium catalysis has surfaced as a uniquely versatile platform for proximal and distal bond functionalizations.[14–16] Hence, we wondered whether position-selective ruthenium-catalyzed C–H phosphorylation would be viable in a position-selectivity-divergent manner by the judicious choice of the reaction conditions. The emergence of electrochemistry applied to organic synthesis has strongly revolutionized molecular synthesis by avoiding the use of chemical oxidants, leading to more sustainable and environmentally friendly synthetic routes,[17] such as in transition metal-catalyzed C–H activation.[18–23]

Electrochemically[24] driven *ortho*-C–H phosphorylation has solely been accomplished with expensive rhodium catalysts[25] or through nickel catalysis, employing high-temperature conditions (110 °C, DG = 8-aminoquinoline).[26] In sharp contrast, studies on metalla-electrocatalyzed C–H phosphorylations with versatile ruthenium catalysts have thus far proven elusive. Herein, we report a mild, electrochemically driven and cost-effective position-selective ruthenaelectro-catalyzed C–H phosphorylation with controlled position-switch from *ortho* to *para*. Moreover, phosphonyl units could be successfully introduced into relevant pharmaceutical compounds *via* late-stage C–H phosphorylation to access structurally diverse active compounds in a single step.

Results and discussion

Reaction optimization of *ortho*-C–H phosphorylation

We initiated our studies by exploring the envisioned ruthenium-electrocatalyzed *ortho*-C–H phosphorylation of arene **1a** and diphenylphosphine oxide **2a** using a graphite felt (GF) and a platinum (Pt) electrode as anode and cathode materials, respectively, in an undivided cell setup (Table 1). The use of [$Ru(OAc)_2$(*p*-cymene)] as the catalyst, in the presence of HFIP as the solvent, led to the formation of the desired phosphorylated product **3a**, with complete *ortho*-selectivity, in 73% isolated yield (entry 1). Several other solvents and bases were also considered, but significantly reduced efficacy was noted (entries 2–3). Furthermore, other transition metal catalysts, such as $Co(OAc)_2 \cdot 4H_2O$, $Cu(OAc)_2$ or $Ni(DME)Cl_2$, gave unsatisfactory results (entry 4). Control experiments demonstrated that electricity is crucial for the C–H phosphorylation (entry 6).

Substrate scope investigation for the *ortho*-C–H phosphorylation

With the optimized reaction conditions in hand, we first investigated the viable scope of the ruthenium-electrocatalyzed *ortho*-C–H phosphorylation (Scheme 2). First, various *N*-substituted arylpurines were probed, including bio-relevant 6-phenylpurine nucleosides, efficiently affording the desired products in good yields (**3a–3d**). Additionally, both electron-withdrawing groups (*e.g.*, –F) and electron-donating groups (*e.g.*, –Me) on the arenes were well tolerated (**3e–3f**). Second, a bipyridine-substituted arene was also tolerated, delivering solely the mono-phosphorylation product (**3g**). Moreover, oxime derivatives selectively delivered the desired product (**3i**). Third, various types of arenes were explored, featuring a wide range of oxazolinyl, pyrazyl or pyridyl substituents (**3j–3n**). Afterwards, the scope of phosphorus coupling partners was further investigated. Fourth, diphenylphosphine oxides bearing electron-donating and electron-withdrawing groups were shown to be suitable coupling partners leading to the formation of the expected products **3o–3s** in good yields. Other pentavalent phosphine oxides, comprised of phenylalkyl phosphine oxides, dithienyl phosphine oxides, and commonly used dimethyl phosphine oxides, in phosphorylated drugs, have been demonstrated to be successful coupling partners (**3t–3w**).

Phosphorylation motifs can confide biological activity to drug molecules.[5] In this context, the direct installation of phosphorylation units into target molecules, accounts for a more sustainable access to structural diversity, facilitating the expansion of the chemical space. Hence, we wondered whether our strategy could be exploited for late-stage C–H phosphorylations. To our delight, diazepam - a therapeutic drug used for acute tension and anxiety states - proved to be an amenable substrate, delivering the desired products **3x–3y** in high yields. Additionally, oxaprozin and 6-phenylpurine riboside, delivered the desired products (**3z–3aa**) with excellent levels of position-selectivity.

Table 1 Optimization of the *ortho*-C–H phosphorylation reaction conditions[a]

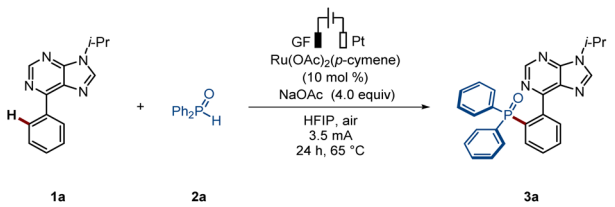

Entry	Deviation from standard conditions	Yield of **3a**[b](%)
1	None	73
2	H_2O/CH_3CN/TFE as solvent	–/–/65
3	Na_2CO_3/Na_3PO_4/NaOPiv as base	62/66/53
4[c]	$Co(OAc)_2 \cdot 4H_2O/Cu(OAc)_2/Ni(DME)Cl_2$	Trace/0/0
5	N_2 instead of air	72
6	Without electricity	0

[a] Reaction conditions **A**: undivided cell, GF anode, Pt cathode, **1a** (0.3 mmol), **2a** (4.0 equiv.), [$Ru(OAc)_2$(*p*-cymene)] (10 mol%), NaOAc (4.0 equiv.), HFIP: 1,1,1,3,3,3-hexafluoropropan-2-ol (3.0 mL), air, 65 °C, 3.5 mA, 24 h. [b] Isolated yields. [c] $Co(OAc)_2 \cdot 4H_2O$ (10 mol%)/$Cu(OAc)_2$ (10 mol%)/$Ni(DME)Cl_2$ (10 mol%).

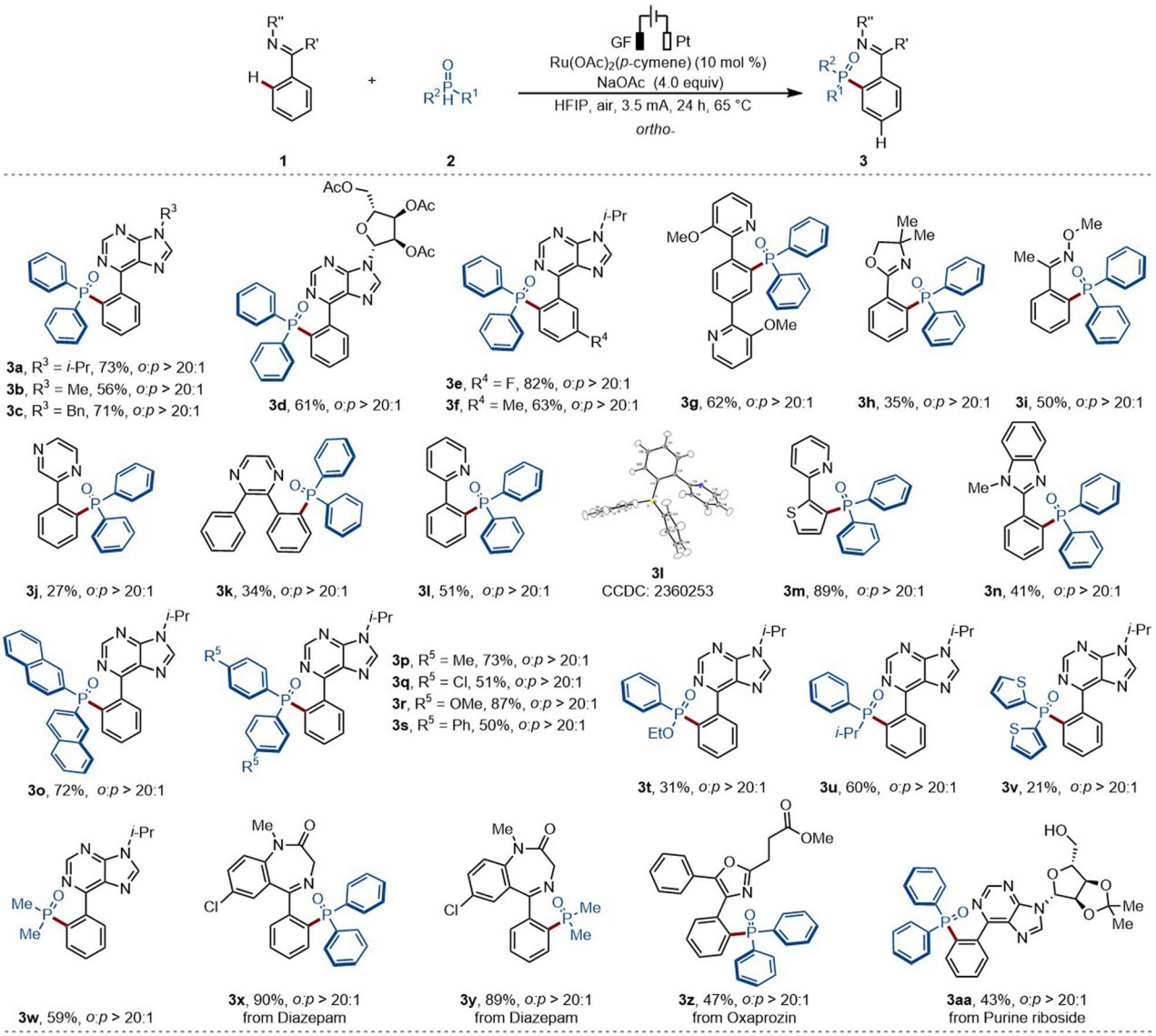

Scheme 2 Scope of the ortho-selective C–H phosphorylation.

Mechanistic studies of *ortho*-C–H phosphorylation

To gain insights into the reaction mechanism, a series of control experiments were conducted. The addition of equimolar amounts of TEMPO resulted in the inhibition of the *ortho*-C–H phosphorylation. However, given that TEMPO is a good reducing agent,[27] such observations do not conclusively support the formation of a *P*-centered radical. Therefore, additional mechanistic experiments were conducted in the presence of representative radical scavengers, including 1,2-diphenylethylene and vinylcyclopropane **6**, which is known to undergo ring opening in the presence of radial species. As a result, the *ortho*-phosphorylation product **3a** was obtained in comparable isolated yields of 63% and 68%, respectively. These findings provide support for a non-radical pathway (Scheme 3a). Next, the addition of D_2O as co-solvent resulted in a H/D scrambling at the *ortho*-position, suggesting a reversible *ortho*-C–H activation (Scheme 3b).

In order to gain insights into the cathodic process, headspace gas chromatography was used and the formation of molecular hydrogen was probed. Thus, we monitored and quantified the formation of molecular hydrogen during the electrocatalytic reaction, which was determined to be 19.8 mL by the end of the electrocatalysis, translating into a faradaic efficiency of 59% (Scheme 3c and ESI Fig. S2, S3†). The result confirmed the hydrogen evolution reaction (HER) as the primary cathodic process, highlighting the unique potential of ruthenium electrocatalysis as a sustainable technology for organic synthesis.

Additionally, cyclic voltammetric (CV) experiments were conducted to assess the redox potential of the substrates as well as the catalyst (Scheme 3d). For the *ortho*-C–H phosphorylation,

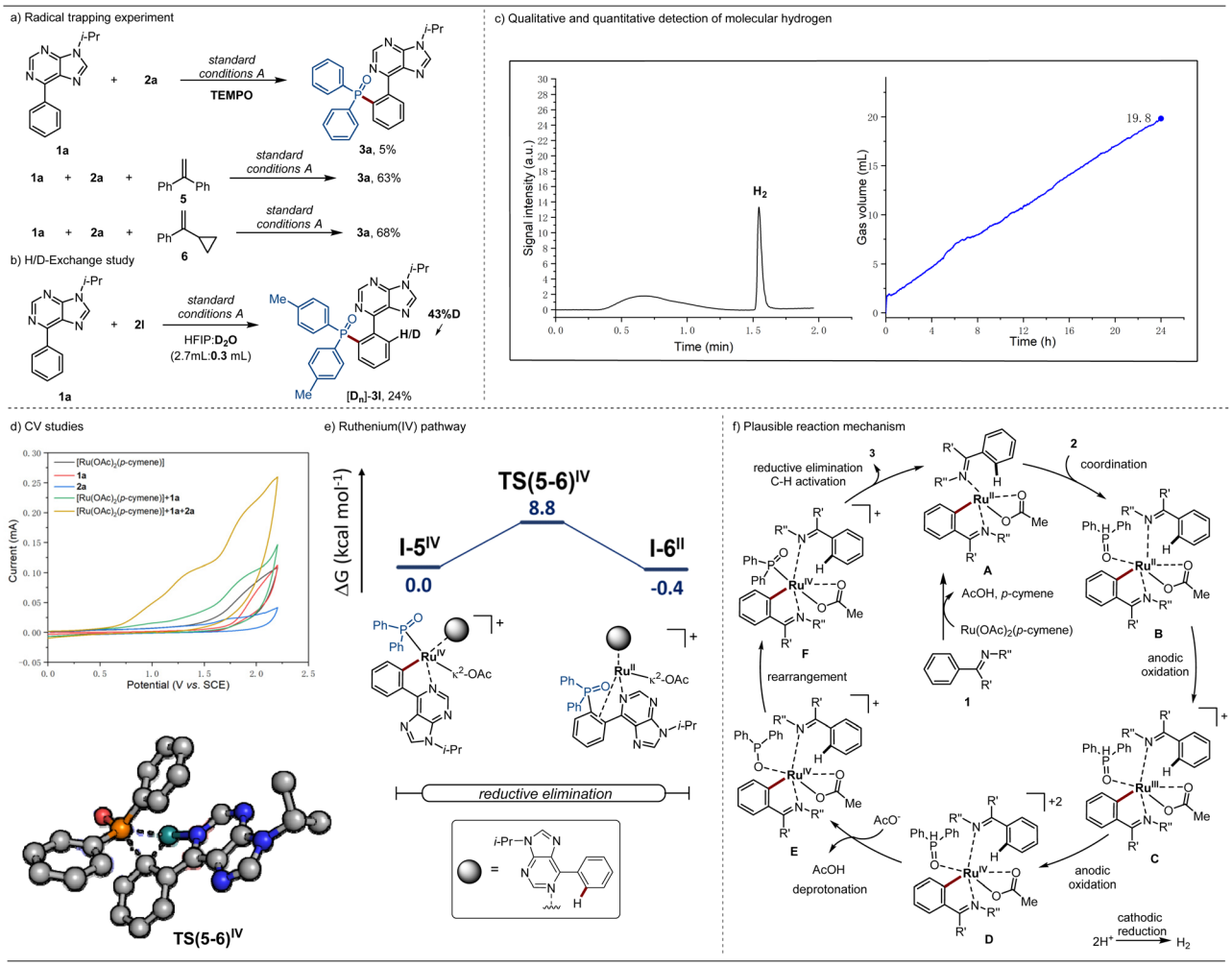

Scheme 3 (a) Radical trapping experiment. (b) H/D-Exchange study. (c) Headspace GC analysis after catalysis (left side) and measurement of gas evolution during catalysis (right side). (d) Cyclic voltammetry studies. (e) Relative Gibbs free energies ($\Delta G_{338.15}$) are given in kcal mol^{-1} for the ruthenium-catalyzed *ortho*-C–H phosphorylation reductive elimination step at the PBE0-D4/def2-TZVPP-SMD(HFIP)//PBE0-D3BJ/def2-SVP level of theory. In the computed transition state structure, non-relevant hydrogens were omitted for clarity. (f) Plausible reaction mechanism for the ruthenaelectro-catalyzed *ortho*-C–H phosphorylation.[27]

the mixture of phenyl-9*H*-purine (**1a**), diphenylphosphine oxide (**2a**), and the catalyst [Ru(OAc)$_2$(*p*-cymene)] exhibited oxidation peaks at $E_{p/2} = 0.95$ V and $E_{p/2} = 1.26$ V *vs.* SCE. These findings are indicative of a ruthenacycle generated after C–H activation being coordinated by SPO **2a**.

The catalyst mode of action for the ruthenium-electrocatalyzed *ortho*-C–H phosphorylation was further investigated through DFT calculations at the PBE0-D4/def2-TZVPP-SMD(HFIP)//PBE0-D3BJ/def2-SVP level of theory (Scheme 3e, Fig. S8 and S9, in the ESI†).[28] Upon phosphine coordination two single electron oxidation steps take place, leading to the formation of the ruthenium(IV) intermediate **I–1^{IV}** (Fig. S8†). Such is consistent with the CV studies, where two oxidation peaks were observed in the presence of phosphine. Subsequently, a facile phosphine deprotonation takes place (**TS(2-3)**) with an energy barrier of 6.8 kcal mol^{-1} giving rise to intermediate **I-3**, which after rearrangement originates a more exergonic intermediate **I-5**. The latter undergoes reductive elimination through transition state **TS(5-6)** with an energy barrier of 8.8 kcal mol^{-1}. Additionally, an alternative pathway for reductive elimination under ruthenium(III) was also investigated (Fig. S9†). The latter has proven to be energetically disfavored, not only by the prohibitive calculated barrier of 40.3 kcal mol^{-1} but also by the formation of an endergonic ruthenium(I) intermediate **I-6^{I}**. Such observations provide support for a ruthenium(III/IV/II) regime.

Based on our experimental and computational mechanistic studies, a plausible reaction mechanism is depicted in Scheme 3f. The *ortho*-phosphorylation commences with the *ortho*-C–H activation, forming the ruthenacycle complex **A**. Subsequently, ligand exchange occurs, leading to a more easily oxidized intermediate **B**, which after two single electron oxidation steps originates the ruthenium(IV) intermediate **D**. Then, deprotonation gives rise to intermediate **E**, which rearranges to form

Table 2 Optimization of the *para*-C–H phosphorylation reaction conditions[a]

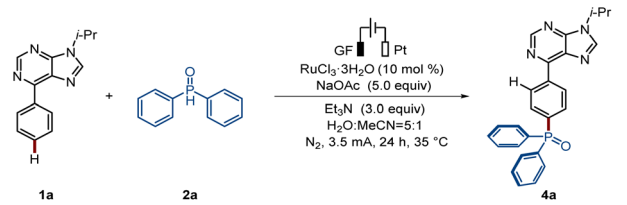

Entry	Deviation from standard conditions	Yield of **4a**[b] (%)
1	None	82
2	Under air	66
3	H_2O/CH_3CN/TFE as solvent	25/12/—
4	Na_2CO_3/Na_3PO_4/NaOPiv as base	78/55/23
5[c]	PPh_3/2,2′-bipyridine as ligand	55/42
6	Without electricity	0

[a] Reaction conditions **B**: undivided cell, GF anode, Pt cathode, **1a** (0.3 mmol), **2a** (4.0 equiv.), [$RuCl_3 \cdot 3H_2O$] (10 mol%), NaOAc (5.0 equiv.), Et_3N (3.0 equiv.), MeCN : H_2O = (0.5 : 2.5 mL), N_2, 35 °C, 3.5 mA, 24 h. [b] Isolated yields. [c] PPh_3 (10 mol%), 2,2′-bipyridine (10 mol%).

intermediate **F**. Finally, **F** undergoes reductive elimination to yield the desired product **3** and to regenerate the active ruthenium(II) catalyst **A**.

Reaction optimization of *para*-C–H phosphorylation

Next, we focused our attention on the envisioned switch towards ruthenaelectro-catalyzed *para*-C–H phosphorylation. We began our studies with arene **1a** and diphenylphosphine oxide **2a** using graphite felt (GF) and platinum (Pt) electrodes as anode and cathode materials, respectively, in an undivided cell setup (Table 2). When $RuCl_3 \cdot 3H_2O$ was used as a catalyst in the presence of MeCN as solvent a minor amount of *para*-C–H phosphorylated product was obtained. Upon further experimentation, the *para*-phosphorylated product **4a** was selectively obtained in an isolated yield of 82% in the presence of $RuCl_3 \cdot 3H_2O$, triethylamine, and a solvent mixture of MeCN and water (Entry 1). Notably, only unconverted substrate **1a** was accounted for in the mass balance here, with no side product, from possible phosphorylation at the purine C–H bond, being detected. Other tested solvents and bases did not improve the efficacy of the reaction (entries 3–4). Moreover, the electricity was shown to be essential for the catalysis to take place (entry 6).

Substrate scope investigation for the *para*-C–H phosphorylation

With the optimized reaction conditions in hand, we directed our attention to the viable substrate scope of the ruthenium-electrocatalyzed *para*-C–H phosphorylation (Scheme 4a). Several *N*-substituted 6-phenylpurines were explored, enabling the formation of the corresponding desired products in good yields with exclusive *para*-selectivity (**4a–4d**). Furthermore, both electron-withdrawing groups (–F) and electron-donating (–Me) on the arenes were well tolerated (**4e–4f**). Diphenylphosphine oxide compounds bearing different substituents (–Cl, –Me, –OMe, $-OCF_3$) were also well tolerated (**4g–4k**). Noticeably, the 1-phenylpyrazole yielded the expected single *para*-C–H phosphorylation product, with no phosphorylation occurring at the pyrazole ring (**4m**). Arenes bearing different substituents, such as pyrimidyl, pyridyl, or tetrazolyl groups, demonstrated higher efficacy, in the absence of triethylamine, with excellent *para*-selectivity (**4o–4q**). Moreover, our approach could be successfully applied to the late-stage C–H phosphorylation of 6-phenylpurine riboside, delivering the desired product (**4r**) with excellent position-selectivity.

Mechanistic studies for the *para*-C–H phosphorylation

To gain mechanistic insights into the ruthenium-electrocatalyzed *para*-C–H phosphorylation, cyclic voltammetry (CV) experiments were conducted to access the redox potential of the substrates as well as the catalyst (Scheme 4b). The Et_3N features an oxidation peak at $E_{p/2} = 0.91$ V *vs.* SCE, which is much lower than the one obtained for **1a**, **2a**, and $RuCl_3 \cdot 3H_2O$, indicating that Et_3N is more susceptible to be oxidized.

Additionally, a series of control experiments were performed. The addition of TEMPO under otherwise identical reaction conditions inhibited the *para*-C–H phosphorylation. Moreover, upon the addition of 1,2-diphenylethylene, the corresponding radical intermediates **7** and **8** were trapped. When vinylcyclopropane **6** was added, the compound resulting from the ring opening (**9**) could be isolated in 70% yield. These findings provide strong support for the involvement of a phosphorus-centered radical in the *para*-phosphorylation (Scheme 4c). However, when D_2O was added to the *para*-phosphorylation reaction, no H/D-scrambling was observed, suggesting that an *ortho*-C–H cycloruthenation is not relevant for the *para*-reaction pathway (Scheme 4d).

Additionally, we monitored and quantified the formation of molecular hydrogen during the electrocatalytic reaction, which was determined to be 26.7 mL by the end of the reaction time, translating into a faradaic efficiency of 68% (Scheme 4e and ESI Fig. S4, S5†). This provides support for the hydrogen evolution reaction (HER) to be the primary cathodic process.

Based on our experimental mechanistic studies, a plausible reaction mechanism is depicted in Scheme 4f. For the *para*-phosphorylation pathway, the nitrogen-containing heteroarene first coordinates to the ruthenium(III) catalyst to form intermediate **G**. Then, $Et_3N^{\cdot+}$ may react with H-phosphonate or H-phosphine oxide to give rise to a phosphorus-centered radical. Subsequently, the electrophilic phosphine radical will attack at the *para*-position of the arene *via* a charge transfer-directed approach,[29] followed by oxidative aromatization to generate the *para*-phosphorylated product. In the meanwhile, at the cathode, protons are reduced to generate molecular hydrogen by HER.

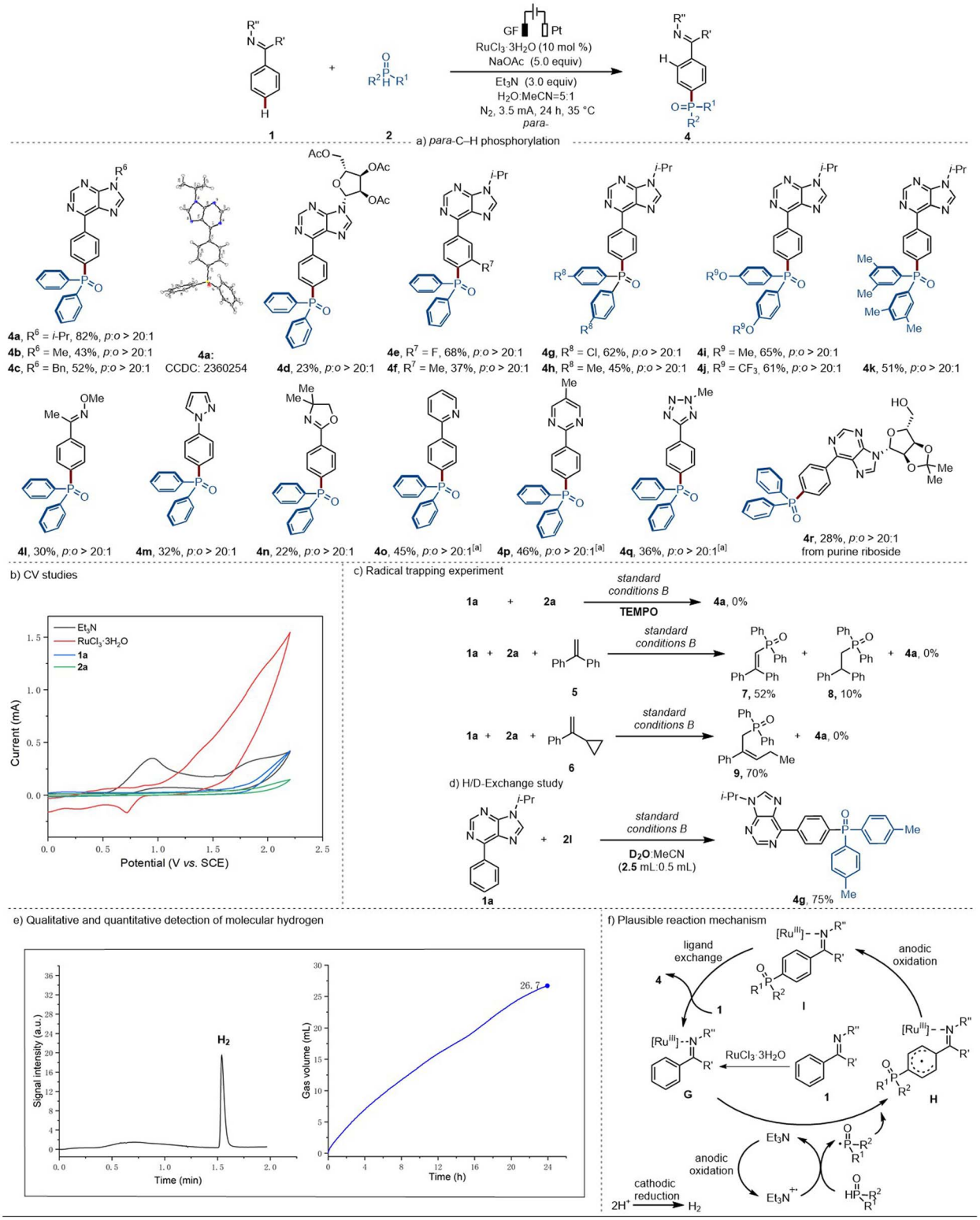

Scheme 4 (a) Scope of the ruthenium-electrocatalyzed *para*-selective C–H phosphorylation, [a]no Et_3N. (b) Cyclic Voltammograms. (c) Radical trapping experiment. Yield ratio calculated by phosphorus NMR from a mixture of **7** and **8**. (d) H/D-exchange study. (e) Headspace GC analysis after catalysis (left side) and measurement of gas evolution during catalysis (right side). (f) Plausible reaction mechanism involved in the ruthenaelectro-catalyzed of *para*-C–H phosphorylation.

Conclusions

In conclusion, we have devised a position-selectivity switch for electrochemical ruthenium-catalyzed C–H phosphorylations enabled by hydrogen evolution reaction (HER). Thereby, we achieved selective *ortho*- and even *para*-C–H phosphorylation. The robustness of the ruthena-electrocatalysis was reflected by a wide substrate scope including various sensitive electrophilic functional groups. Our strategy thereby enabled challenging late-stage phosphorylations of biorelevant pharmaceuticals. Experimental and computational mechanistic studies provided strong support for an unusual ruthenium(III/IV/II) manifold for the ruthenaelectro-catalyzed proximal phosphorylation.

Data availability

All data associated with this study are available in the article and ESI.†

Author contributions

Conceptualization, L. A.; methodology, X.-Y. G.; investigation, X.-Y. G.; DFT calculation, J. C. A. O.; cyclic voltammetry studies, S. L. H.; headspace GC analysis and measurement, S .T.; HRMS studies, T. v. M.; writing – original Draft, X.-Y. G., B.-S. Z. and J. C. A. O.; writing – review & editing, X.-Y. G., J. C. A. O., and S. C.; funding acquisition, L. A.; resources, L. A.; supervision, L. A.

Conflicts of interest

There are no conflicts to declare.

Acknowledgements

The authors gratefully acknowledge support from the ERC Advanced grant no. 101021358, the DFG (Gottfried Wilhelm Leibniz award to L. A., SPP2363). We thank Dr Christopher Golz (University of Göttingen) for the assistance with the X-ray diffraction analysis,[30] Dr Holm Frauendorf for HRMS analysis and Dr Michael John for NMR spectroscopy.

Notes and references

1 (*a*) C. S. Demmer, N. Krogsgaard-Larsen and L. Bunch, Review on Modern Advances of Chemical Methods for the Introduction of a Phosphonic Acid Group, *Chem. Rev.*, 2011, **111**, 7981–8006; (*b*) Y.-Y. Zhu, T. Zhang, L. Zhou and S.-D. Yang, Concise synthesis of N-phosphorylated amides through three-component reactions, *Green Chem.*, 2021, **23**, 9417–9421.

2 T. D. Baguley, H.-C. Xu, M. Chatterjee, A. C. Nairn, P. J. Lombroso and J. A. Ellman, Substrate-Based Fragment Identification for the Development of Selective, Nonpeptidic Inhibitors of Striatal-Enriched Protein Tyrosine Phosphatase, *J. Med. Chem.*, 2013, **56**, 7636–7650.

3 K. J. Gagnon, H. P. Perry and A. Clearfield, Conventional and Unconventional Metal–Organic Frameworks Based on Phosphonate Ligands: MOFs and UMOFs, *Chem. Rev.*, 2012, **112**, 1034–1054.

4 (*a*) J. Holz, H. Jiao, M. Gandelman and A. Börner, About the Inversion Barriers of P-Chirogenic Triaryl-Substituted Phosphanes, *Eur. J. Org Chem.*, 2018, 2984–2994; (*b*) Y.-N. Ma, S.-X. Li and S.-D. Yang, New Approaches for Biaryl-Based Phosphine Ligand Synthesis *via* P═O Directed C–H Functionalizations, *Acc. Chem. Res.*, 2017, **50**, 1480–1492.

5 C. A. Tian and C. C. Chiu, Importance of Hydrophilic Groups on Modulating the Structural, Mechanical, and Interfacial Properties of Bilayers: A Comparative Molecular Dynamics Study of Phosphatidylcholine and Ion Pair Amphiphile Membranes, *Int. J. Mol. Sci.*, 2018, **19**, 1552–1571.

6 P. S. Shirude, A. K. K. Chattopadhyay, K. Ellen and N. R. Wurtz, Biaryl dialkyl phosphine oxide Fpr2 agonists, WO2020257161A1, 2020.

7 (*a*) J. Zhao, Z. Feng, D. Zhong, X. Yang, Y. Wu, G. Zhou and Z. Wu, Cyclometalated Platinum Complexes with Aggregation-Induced Phosphorescence Emission Behavior and Highly Efficient Electroluminescent Ability, *Chem. Mater.*, 2018, **30**, 929–946; (*b*) G. Sarada, A. Maheshwaran, W. Cho, T. Lee, S. H. Han, J. Y. Lee and S.-H. Jin, Pure blue phosphorescence by new N-heterocyclic carbene-based Ir(III) complexes for organic light-emitting diode application, *Dyes Pigm.*, 2018, **150**, 1–8.

8 (*a*) J. H. Docherty, T. M. Lister, G. McArthur, M. T. Findlay, P. Domingo-Legarda, J. Kenyon, S. Choudhary and I. Larrosa, Transition-Metal-Catalyzed C–H Bond Activation for the Formation of C–C Bonds in Complex Molecules, *Chem. Rev.*, 2023, **123**, 7692–7760; (*b*) T. Rogge, N. Kaplaneris, N. Chatani, J. Kim, S. Chang, B. Punji, L. L. Schafer, D. G. Musaev, J. Wencel-Delord, C. A. Roberts, R. Sarpong, Z. E. Wilson, M. A. Brimble, M. J. Johansson and L. Ackermann, C–H activation, *Nat. Rev. Methods Primers*, 2021, **1**, 43; (*c*) U. Dutta, S. Maiti, T. Bhattacharya and D. Maiti, Arene diversification through distal C(sp^2)–H functionalization, *Science*, 2021, **372**, eabd5992; (*d*) R. R. Karimov and J. F. Hartwig, Transition-Metal-Catalyzed Selective Functionalization of C(sp^3)–H Bonds in Natural Products, *Angew. Chem., Int. Ed.*, 2018, **57**, 4234–4241; (*e*) Z. Zhang, K. Tanaka and J.-Q. Yu, Remote site-selective C–H activation directed by a catalytic bifunctional template, *Nature*, 2017, **543**, 538–542; (*f*) H. M. L. Davies, J. Du Bois and J.-Q. Yu, C–H Functionalization in organic synthesis, *Chem. Soc. Rev.*, 2011, **40**, 1855–1856; (*g*) L. Ackermann, Carboxylate-Assisted Transition-Metal-Catalyzed C–H Bond Functionalizations: Mechanism and Scope, *Chem. Rev.*, 2011, **111**, 1315–1345.

9 C.-G. Feng, M. Ye, K.-J. Xiao, S. Li and J.-Q. Yu, Pd(II)-Catalyzed Phosphorylation of Aryl C–H Bonds, *J. Am. Chem. Soc.*, 2013, **135**, 9322–9325.

10 (*a*) M. Min, D. Kang, S. Jung and S. Hong, Rhodium-Catalyzed Direct C–H Phosphorylation of (Hetero)arenes Suitable for Late-Stage Functionalization, *Adv. Synth. Catal.*, 2016, **358**, 1296–1301; (*b*) C. Li, T. Yano, N. Ishida

and M. Murakami, Pyridine-Directed Palladium-Catalyzed Phosphonation of C(sp^2)-H Bonds, *Angew. Chem., Int. Ed.*, 2013, **52**, 9801–9804.

11 S. Wang, R. Guo, G. Wang, S.-Y. Chen and X.-Q. Yu, Copper-catalyzed phosphorylation of sp^2 C–H bonds, *Chem. Commun.*, 2014, **50**, 12718–12721.

12 (*a*) O. Berger and J.-L. Montchamp, Manganese-Catalyzed and Mediated Synthesis of Arylphosphinates and Related Compounds, *J. Org. Chem.*, 2019, **84**, 9239–9256; (*b*) L. Niu, J. Liu, H. Yi, S. Wang, X.-A. Liang, A. K. Singh, C.-W. Chiang and A. Lei, Visible-Light-Induced External Oxidant-Free Oxidative Phosphonylation of C(sp^2)–H Bonds, *ACS Catal.*, 2017, **7**, 7412–7416; (*c*) O. Berger and J.-L. Montchamp, Manganese-Mediated Homolytic Aromatic Substitution with Phosphinylidenes, *Chem. Rec.*, 2017, **17**, 1203–1212.

13 (*a*) N. Sabat, L. Poštová Slavětínská, B. Klepetářová and M. Hocek, C–H Phosphonation of Pyrrolopyrimidines: Synthesis of Substituted 7- and 9-Deazapurine-8-phosphonate Derivatives, *J. Org. Chem.*, 2016, **81**, 9507–9514; (*b*) C.-B. Xiang, Y.-J. Bian, X.-R. Mao and Z.-Z. Huang, Coupling Reactions of Heteroarenes with Phosphites under Silver Catalysis, *J. Org. Chem.*, 2012, **77**, 7706–7710.

14 (*a*) O. M. Ogba, N. C. Warner, D. J. O'Leary and R. H. Grubbs, Recent advances in ruthenium-based olefin metathesis, *Chem. Soc. Rev.*, 2018, **47**, 4510–4544; (*b*) L. Ackermann, Carboxylate-Assisted Ruthenium-Catalyzed Alkyne Annulations by C–H/Het–H Bond Functionalizations, *Acc. Chem. Res.*, 2014, **47**, 281–295; (*c*) P. B. Arockiam, C. Bruneau and P. H. Dixneuf, Ruthenium(II)-Catalyzed C–H Bond Activation and Functionalization, *Chem. Rev.*, 2012, **112**, 5879–5918; (*d*) L. Ackermann and R. J. C. A. Vicente, Ruthenium-catalyzed direct arylations through C–H bond cleavages, *Top. Curr. Chem.*, 2010, **292**, 211–229; (*e*) R. Noyori and S. Hashiguchi, Asymmetric Transfer Hydrogenation Catalyzed by Chiral Ruthenium Complexes, *Acc. Chem. Res.*, 1997, **30**, 97–102.

15 (*a*) G.-W. Wang, M. Wheatley, M. Simonetti, D. M. Cannas and I. Larrosa, Cyclometalated Ruthenium Catalyst Enables Ortho-Selective C–H Alkylation with Secondary Alkyl Bromides, *Chem*, 2020, **6**, 1459–1468; (*b*) W.-T. Fan, Y. Li, D. Wang, S.-J. Ji and Y. Zhao, Iron-Catalyzed Highly *para*-Selective Difluoromethylation of Arenes, *J. Am. Chem. Soc.*, 2020, **142**, 20524–20530; (*c*) X.-G. Wang, Y. Li, H.-C. Liu, B.-S. Zhang, X.-Y. Gou, Q. Wang, J.-W. Ma and Y.-M. Liang, Three-Component Ruthenium-Catalyzed Direct Meta-Selective C–H Activation of Arenes: A New Approach to the Alkylarylation of Alkenes, *J. Am. Chem. Soc.*, 2019, **141**, 13914–13922; (*d*) M. Simonetti, D. M. Cannas, X. Just-Baringo, I. J. Vitorica-Yrezabal and I. Larrosa, Cyclometallated ruthenium catalyst enables late-stage directed arylation of pharmaceuticals, *Nat. Chem.*, 2018, **10**, 724–731; (*e*) G. Li, D. Li, J. Zhang, D.-Q. Shi and Y. Zhao, Ligand-Enabled Regioselectivity in the Oxidative Cross-coupling of Arenes with Toluenes and Cycloalkanes Using Ruthenium Catalysts: Tuning the Site-Selectivity from the ortho to meta Positions, *ACS Catal.*, 2017, **7**, 4138–4143; (*f*) J. A. Leitch and C. G. Frost, Ruthenium-catalysed σ-activation for remote meta-selective C–H functionalisation, *Chem. Soc. Rev.*, 2017, **46**, 7145–7153; (*g*) C. J. Teskey, A. Y. W. Lui and M. F. Greaney, Ruthenium-Catalyzed meta-Selective C-H Bromination, *Angew. Chem., Int. Ed.*, 2015, **54**, 11677–11680.

16 (*a*) L. Guillemard, L. Ackermann and M. J. Johansson, Late-stage meta-C–H alkylation of pharmaceuticals to modulate biological properties and expedite molecular optimisation in a single step, *Nat. Commun.*, 2024, **15**, 3349–3358; (*b*) K. Korvorapun, M. Moselage, J. Struwe, T. Rogge, A. M. Messinis and L. Ackermann, Regiodivergent C−H and Decarboxylative C−C Alkylation by Ruthenium Catalysis: ortho *versus* meta Position-Selectivity, *Angew. Chem., Int. Ed.*, 2020, **59**, 18795–18803; (*c*) P. Gandeepan, J. Koeller, K. Korvorapun, J. Mohr and L. Ackermann, Visible-Light-Enabled Ruthenium-Catalyzed meta-C−H Alkylation at Room Temperature, *Angew. Chem., Int. Ed.*, 2019, **58**, 9820–9825; (*d*) J. Li, K. Korvorapun, S. De Sarkar, T. Rogge, D. J. Burns, S. Warratz and L. Ackermann, Ruthenium(II)-catalysed remote C–H alkylations as a versatile platform to meta-decorated arenes, *Nat. Commun.*, 2017, **8**, 15430; (*e*) N. Hofmann and L. Ackermann, meta-Selective C–H Bond Alkylation with Secondary Alkyl Halides, *J. Am. Chem. Soc.*, 2013, **135**, 5877–5884; (*f*) L. Ackermann, P. Novák, R. Vicente and N. Hofmann, Ruthenium-Catalyzed Regioselective Direct Alkylation of Arenes with Unactivated Alkyl Halides through C-H Bond Cleavage, *Angew. Chem., Int. Ed.*, 2009, **48**, 6045–6048.

17 (*a*) M. Y. Gao and C. J. I. J. O. C. Gosmini, Transition Metal-Catalyzed Electroreductive Cross-Couplings for C− C Bond Formation, *Isr. J. Chem.*, 2024, **64**, e202300074; (*b*) L. Ackermann, R. C. D. Brown, P. Enders, P. Fang, A. A. Folgueiras-Amador, R. Francke, J. Galczynski, C. Gosmini, J. W. Hodgson, Z. W. Hou, H. Huang, Z. Huang, S. Inagi, K. Kuciński, M. Kuriyama, K. Lam, T. H. Lambert, M. C. Leech, A. J. J. Lennox, Z. Lin, R. D. Little, L. Massignan, T. S. Mei, T. H. Meyer, K. D. Moeller, O. Onomura, A. Prudlik, Z. Ruan, A. Scheremetjew, P. Schiltz, M. Selt, E. Villani, S. R. Waldvogel, Z. H. Wang, T. Wu, Y. K. Xing, H. C. Xu and K. Yamamoto, *Electrochemistry in Organic Synthesis*, 2022, DOI: **10.1055/b000000126**; (*c*) J. C. Siu, N. Fu and S. Lin, Catalyzing Electrosynthesis: A Homogeneous Electrocatalytic Approach to Reaction Discovery, *Acc. Chem. Res.*, 2020, **53**, 547–560; (*d*) T. H. Meyer, I. Choi, C. Tian and L. Ackermann, Powering the Future: How Can Electrochemistry Make a Difference in Organic Synthesis?, *Chem*, 2020, **6**, 2484–2496; (*e*) C. Kingston, M. D. Palkowitz, Y. Takahira, J. C. Vantourout, B. K. Peters, Y. Kawamata and P. S. Baran, A Survival Guide for the "Electro-curious", *Acc. Chem. Res.*, 2020, **53**, 72–83; (*f*) Y. Yuan and A. Lei, Electrochemical Oxidative Cross-Coupling with Hydrogen Evolution Reactions, *Acc. Chem. Res.*, 2019, **52**, 3309–3324;

(*g*) P. Xiong and H.-C. Xu, Chemistry with Electrochemically Generated N-Centered Radicals, *Acc. Chem. Res.*, 2019, **52**, 3339–3350; (*h*) S. Möhle, M. Zirbes, E. Rodrigo, T. Gieshoff, A. Wiebe and S. R. Waldvogel, Modern Electrochemical Aspects for the Synthesis of Value-Added Organic Products, *Angew. Chem., Int. Ed.*, 2018, **57**, 6018–6041; (*i*) M. Yan, Y. Kawamata and P. S. Baran, Synthetic Organic Electrochemical Methods Since 2000: On the Verge of a Renaissance, *Chem. Rev.*, 2017, **117**, 13230–13319.

18 (*a*) E. M. Alvarez, G. Stewart, M. Ullah, R. Lalisse, O. Gutierrez and C. A. Malapit, Site-Selective Electrochemical Arene C–H Amination, *J. Am. Chem. Soc.*, 2024, **146**, 3591–3597; (*b*) Y. Gao, B. Zhang, J. He and P. S. Baran, Ni-Electrocatalytic Enantioselective Doubly Decarboxylative $C(sp^3)$–$C(sp^3)$ Cross-Coupling, *J. Am. Chem. Soc.*, 2023, **145**, 11518–11523; (*c*) T. S.-B. Lou, Y. Kawamata, T. Ewing, G. A. Correa-Otero, M. R. Collins and P. S. Baran, Scalable, Chemoselective Nickel Electrocatalytic Sulfinylation of Aryl Halides with SO2, *Angew. Chem., Int. Ed.*, 2022, **61**, e202208080; (*d*) M. Saito, Y. Kawamata, M. Meanwell, R. Navratil, D. Chiodi, E. Carlson, P. Hu, L. Chen, S. Udyavara, C. Kingston, M. Tanwar, S. Tyagi, B. P. McKillican, M. G. Gichinga, M. A. Schmidt, M. D. Eastgate, M. Lamberto, C. He, T. Tang, C. A. Malapit, M. S. Sigman, S. D. Minteer, M. Neurock and P. S. Baran, N-Ammonium Ylide Mediators for Electrochemical C–H Oxidation, *J. Am. Chem. Soc.*, 2021, **143**, 7859–7867.

19 (*a*) Z.-W. Hou, H. Yan, J. Song and H.-C. Xu, Photoelectrocatalytic C–H amination of arenes, *Green Chem.*, 2023, **25**, 7959–7962; (*b*) N. Chen and H.-C. Xu, Electrochemically Driven Radical Reactions: From Direct Electrolysis to Molecular Catalysis, *Chem. Rec.*, 2021, **21**, 2306–2319; (*c*) P. Xu, P.-Y. Chen and H.-C. Xu, Scalable Photoelectrochemical Dehydrogenative Cross-Coupling of Heteroarenes with Aliphatic C−H Bonds, *Angew. Chem., Int. Ed.*, 2020, **59**, 14275–14280; (*d*) X.-L. Lai, X.-M. Shu, J. Song and H.-C. Xu, Electrophotocatalytic Decarboxylative C−H Functionalization of Heteroarenes, *Angew. Chem., Int. Ed.*, 2020, **59**, 10626–10632; (*e*) F. Xu, Y.-J. Li, C. Huang and H.-C. Xu, Ruthenium-Catalyzed Electrochemical Dehydrogenative Alkyne Annulation, *ACS Catal.*, 2018, **8**, 3820–3824.

20 (*a*) Y. Yuan, J. Yang and A. Lei, Recent advances in electrochemical oxidative cross-coupling with hydrogen evolution involving radicals, *Chem. Soc. Rev.*, 2021, **50**, 10058–10086; (*b*) X. Hu, L. Nie, G. Zhang and A. Lei, Electrochemical Oxidative [4+2] Annulation for the π-Extension of Unfunctionalized Heterobiaryl Compounds, *Angew. Chem., Int. Ed.*, 2020, **59**, 15238–15243; (*c*) X. Hu, G. Zhang, L. Nie, T. Kong and A. Lei, Electrochemical oxidation induced intermolecular aromatic C-H imidation, *Nat. Commun.*, 2019, **10**, 5467–5476; (*d*) X. Hu, G. Zhang, F. Bu, L. Nie and A. Lei, Electrochemical-Oxidation-Induced Site-Selective Intramolecular $C(sp^3)$–H Amination, *ACS Catal.*, 2018, **8**, 9370–9375.

21 (*a*) Y.-K. Xing, Z.-H. Wang, P. Fang, C. Ma and T.-S. Mei, Divergent synthesis of aryl amines and dihydroquinazolinones *via* electrochemistry-enabled rhodium-catalyzed C–H functionalization, *Sci. China:Chem.*, 2023, **66**, 2863–2870; (*b*) D. Liu, Z.-R. Liu, Z.-H. Wang, C. Ma, S. Herbert, H. Schirok and T.-S. Mei, Paired electrolysis-enabled nickel-catalyzed enantioselective reductive cross-coupling between α-chloroesters and aryl bromides, *Nat. Commun.*, 2022, **13**, 7318–7326; (*c*) K.-J. Jiao, Y.-K. Xing, Q.-L. Yang, H. Qiu and T.-S. Mei, Site-Selective C–H Functionalization *via* Synergistic Use of Electrochemistry and Transition Metal Catalysis, *Acc. Chem. Res.*, 2020, **53**, 300–310.

22 (*a*) T. Michiyuki, I. Maksso and L. Ackermann, Photo-Induced Ruthenium-Catalyzed C−H Arylation Polymerization at Ambient Temperature, *Angew. Chem., Int. Ed.*, 2024, e202400845; (*b*) Z. Lin, J. C. A. Oliveira, A. Scheremetjew and L. Ackermann, Palladium-Catalyzed Electrooxidative Double C–H Arylation, *J. Am. Chem. Soc.*, 2024, **146**, 228–239; (*c*) Y. Wang, S. Dana, H. Long, Y. Xu, Y. Li, N. Kaplaneris and L. Ackermann, Electrochemical Late-Stage Functionalization, *Chem. Rev.*, 2023, **123**, 11269–11335; (*d*) T. von Münchow, S. Dana, Y. Xu, B. Yuan and L. Ackermann, Enantioselective electrochemical cobalt-catalyzed aryl C–H activation reactions, *Science*, 2023, **379**, 1036–1042; (*e*) Y. Li, S. Dana and L. Ackermann, Recent advances in organic electrochemical functionalizations for specialty chemicals, *Curr. Opin. Electrochem.*, 2023, **40**, 101312; (*f*) Y. Wang, H. Simon, X. Chen, Z. Lin, S. Chen and L. Ackermann, Distal Ruthenaelectro-Catalyzed meta-C−H Bromination with Aqueous HBr, *Angew. Chem., Int. Ed.*, 2022, **61**, e202201595; (*g*) X. Tan, X. Hou, T. Rogge and L. Ackermann, Ruthenaelectro-Catalyzed Domino Three-Component Alkyne Annulation for Expedient Isoquinoline Assembly, *Angew. Chem., Int. Ed.*, 2021, **60**, 4619–4624; (*h*) L. Ackermann, Metalla-electrocatalyzed C–H Activation by Earth-Abundant 3d Metals and Beyond, *Acc. Chem. Res.*, 2020, **53**, 84–104.

23 (*a*) J. Qi, J. Xu, H. T. Ang, B. Wang, N. K. Gupta, S. R. Dubbaka, P. O'Neill, X. Mao, Y. Lum and J. Wu, Electrophotochemical Synthesis Facilitated Trifluoromethylation of Arenes Using Trifluoroacetic Acid, *J. Am. Chem. Soc.*, 2023, **145**, 24965–24971; (*b*) H. Huang, K. A. Steiniger and T. H. Lambert, Electrophotocatalysis: Combining Light and Electricity to Catalyze Reactions, *J. Am. Chem. Soc.*, 2022, **144**, 12567–12583; (*c*) S. Jin, J. Kim, D. Kim, J.-W. Park and S. Chang, Electrolytic C–H Oxygenation *via* Oxidatively Induced Reductive Elimination in Rh Catalysis, *ACS Catal.*, 2021, **11**, 6590–6595; (*d*) M.-J. Luo, M. Hu, R.-J. Song, D.-L. He and J.-H. Li, Ruthenium(ii)-catalyzed electrooxidative [4+2] annulation of benzylic alcohols with internal alkynes: entry to isocoumarins, *Chem. Commun.*, 2019, **55**, 1124–1127.

24 (*a*) S. Wang, Q. Xue, Z. Guan, Y. Ye and A. Lei, *ACS Catal.*, 2021, **11**, 4295–4300; (*b*) Y. Kurimoto, J. Yamashita, K. Mitsudo, E. Sato and S. Suga, *Org. Lett.*, 2021, **23**, 3120–3124; (*c*) K.-J. Li, Y.-Y. Jiang, K. Xu, C.-C. Zeng and B.-G. Sun, *Green Chem.*, 2019, **21**, 4412–4421.

25 Z.-J. Wu, F. Su, W. Lin, J. Song, T.-B. Wen, H.-J. Zhang and H.-C. Xu, Scalable Rhodium(III)-Catalyzed Aryl C−H Phosphorylation Enabled by Anodic Oxidation Induced Reductive Elimination, *Angew. Chem., Int. Ed.*, 2019, **58**, 16770–16774.
26 S.-K. Zhang, A. Del Vecchio, R. Kuniyil, A. M. Messinis, Z. Lin and L. Ackermann, Electrocatalytic C–H phosphorylation through nickel(III/IV/II) catalysis, *Chem*, 2021, **7**, 1379–1392.
27 X.-Y. Qian, S.-Q. Li, J. Song and H.-C. Xu, TEMPO-Catalyzed Electrochemical C–H Thiolation: Synthesis of Benzothiazoles and Thiazolopyridines from Thioamides, *ACS Catal.*, 2017, **7**, 2730–2734.
28 For detailed information see ESI.†
29 G. B. Boursalian, W. S. Ham, A. R. Mazzotti and T. Ritter, Charge-transfer-directed radical substitution enables *para*-selective C–H functionalization, *Nat. Chem.*, 2016, **8**, 810–815.
30 For X-ray single crystal diffraction data: (*a*) CCDC 2360253: Experimental Crystal Structure Determination, 2024, DOI: 10.5517/ccdc.csd.cc2k7162; ; (*b*) CCDC 2360254: Experimental Crystal Structure Determination, 2024, DOI: 10.5517/ccdc.csd.cc2k7173.